Sensors & Actuators: B. Chemical 423 (2025) 136840

Contents lists available at ScienceDirect

Sensors and Actuators: B. Chemical

journal homepage: www.elsevier.com/locate/snb

In-capillary magnetic separation and enrichment coupled with laser-induced fluorescence for rapid determination of biomolecules

Shu-Ting Cheng, Rong-Rong Meng, Yue-Hong Pang, Xiao-Fang Shen *

School of Food Science and Technology, Jiangnan University, Wuxi 214122, China

ARTICLE INFO

Keywords:
Capillary
Magnetic separation
Enrichment
Laser-induced fluorescence
Biomolecules

ABSTRACT

Biomolecules are indispensable in the life activities and metabolism of various organisms, and their highly sensitive detection is of great significance for disease diagnosis and food safety. Due to the complexity of the matrix and the low concentration of the target, separation and enrichment of biomolecules prior to detection are necessary and time-consuming. Herein, a novel approach combining in-capillary magnetic separation and enrichment with laser-induced fluorescence detection method was proposed for qualitative and quantitative analysis of biomolecules. Two different sequence aptamers modified with magnetic nanoparticles and labeled with fluorescence were used as capture probes and signal probes to form sandwich structures with target molecules for detection. Under the combined influence of magnetic field force and fluid drag force, the integration of separation, enrichment and on-line detection were finished within 5 min. Under optimal conditions, the developed method provided a low limit of detection as 2.7 fmol/L, 0.57 nmol/L, 3 CFU/mL for DNA, thrombin and *Staphylococcus aureus*, respectively. This proposed method offers a promising platform for the sensitive and rapid determination of biomolecules. It holds significant potential for future applications in fields of environmental and biochemical analysis.

1. Introduction

Biomolecules, an integral part of organisms, play a crucial role in the normal growth, life activities and metabolism. The sensitive detection of biomolecules is an important demand in the fields of clinical diagnosis, environmental monitoring and food safety [1–3]. Clinical biomolecules, including small molecules, nucleic acids and proteins, are fundamental for understanding their biological and physiological functions and for developing clinical diagnostics [4,5]. These molecules exhibit diverse biological functions, including the storage and transmission of genetic information, regulation of biological activities, transportation of small molecules, and catalysis of reactions [6–8]. When large-scale infectious diseases occur frequently, it is essential to diagnose patients with infectious diseases as early as possible, and conduct clinical observations to control them to prevent the spread of infectious diseases [9,10]. The high efficiency and accuracy of biomolecule detection have become a bottleneck restricting the development of rapid detection technology for DNA, viruses and other biomolecules.

The content of most biomolecules is particularly low in situations involving disease diagnosis and food safety. To improve the sensitivity of detection, it is essential to increase the number of target biomolecules per unit volume [11]. At present, there are several DNA amplification techniques available, such as recombinase polymerase amplification (RPA), rolling circle amplification (RCA), loop-mediated isothermal amplification (LAMP), polymerase chain reaction (PCR), hybridization chain reaction (HCR) and so on [12–14]. In PCR, the target DNA fragments can be amplified in large quantities through the cycle of denaturation, annealing and polymerization under the action of DNA polymerase [15]. Since the concentration of many protein molecules in the body is very low, signal amplification is a key issue during the detection of low-abundance proteins [16,17]. Nevertheless, enriching low-abundance proteins greatly increases the probability of identification and allows for the effective identification of proteins that are not easily detected [18,19]. Traditional methods for detecting bacteria often involve time-consuming steps such as bacterial proliferation, separation, and purification in the culture medium, especially the long cycle of bacterial proliferation [20,21]. Moreover, these operations are relatively cumbersome and prone to interference from other factors, making them unsuitable for timely and rapid evaluation of biomolecules.

The detection of biomolecules is often complicated by their presence

* Corresponding author.
E-mail address: xfshen@jiangnan.edu.cn (X.-F. Shen).

https://doi.org/10.1016/j.snb.2024.136840
Received 30 July 2024; Received in revised form 10 October 2024; Accepted 23 October 2024
Available online 24 October 2024

in complex biological matrices, including blood, bodily fluids, and food products. Prior to analysis, these molecules must undergo separation to ensure accurate results [22]. Several methods can be used to separate biomolecules, such as electrophoresis, capillary electrophoresis and liquid chromatography mass spectrometry [23–25]. Separation and enrichment technology can improve sensitivity, selectivity and accuracy [26,27]. Magnetic nanoparticles functionalized with antibodies or aptamers have been used in the pretreatment for the separation and enrichment of target in samples. Liang et. al prepared amino group-functionalized silica-coated magnetic nanoparticles as both immobilization matrix and separation tool, utilizing surface-enhanced Raman scattering (SERS) for the detection of DNA sequences related to HIV [28]. Zhao et. al constructed an aptasensor using Fe_3O_4@Au-Apt as a nanoprobe to separate *Staphylococcus aureus* (*S. aureus*), and conducted specific SERS detection [29]. Du et. al designed cleavable amino-oxy-functionalized Fe_3O_4 magnetic nanoparticles for the rapid and selective separation of sialo-glycoproteins, followed by tandem mass spectrometry for analysis and detection [30]. Nevertheless, the separation and detection of targets are carried out in several steps, requiring corresponding instruments for detection. To improve sensitivity and efficiency of enrichment, it is necessary to simplify operating steps to achieve integration. Therefore, establishing a new method for biomolecule determination that enables rapid separation, enrichment, and increases concentration per unit volume is essential.

In order to enrich and capture biomolecules, aptamers were used to modify magnetic nanoparticles. The target biomolecules were selectively labeled, the aptamers were labeled with fluorescent molecules to provide a more sensitive and selective signal [31]. Capillary is usually used for electrophoresis or capillary gas chromatography [32,33], we used it for in-line enrichment in this work. Biomolecules were introduced into capillary, and a magnetic field was applied to it. When the magnetic nanoparticles passed by, the targets attracted them, achieving in-line enrichment. Coupled with laser-induced fluorescence (LIF), one of the most sensitive methods, capillary electrophoresis shows a sensitive signal with low background noise and minimal sample consumption [34–36].

In this work, we introduced an innovative method that integrates in-capillary magnetic separation and enrichment with LIF detection for the qualitative and quantitative detection of biomolecules. Under the combined influence of magnetic field force and fluid drag force, this method can achieve the integration of separation, enrichment, and on-line detection of biomolecules represented by DNA and thrombin, and can even be extended to *S. aureus*.

2. Experimental

2.1. Materials and reagents

Amino coated γ-Fe_2O_3 (MNPs, an average diameter of 10 nm) were purchased from Nanjing Nonoeast Biotech Co., Ltd. (Nanjing, China). All the reagents for the buffers and glutaraldehyde (25 %, V/V) were obtained from Sinopharm Chemical Reagent Co., Ltd. (Shanghai, China). Thrombin was purchased from Genetimes Biological Technology Co., Ltd. (Nanjing, China). Bovine serum was obtained from Zhejiang Tianhang Biotechnology Co., Ltd. (Huzhou, China). *S. aureus*, *Escherichia coli* (*E. coli*), *Salmonella*, *Shigella dysenteriae*, *Vibrio parahaemolyticus* and *Bacillus cereus* were provided from the American Type Culture Collection. The avidin (streptavidin) and aptamers used in experiment were obtained by Shanghai Sangon Biological Engineering Technology & Services Co., Ltd. (Shanghai, China) and the following sequences are provided in Table S1. Fused-silica capillary (ID: 250 μm) were from Ruifeng chromatographic devices company Co. Ltd. (Handan, China). Water phase needle filter membrane (0.45 μm aperture) was purchased from Tianjin Fuji Technology Co., Ltd (Tianjin, China). Water (18.2 MΩ) used in all experiments was prepared using a compact ultrapure water system from Barnstead (Dubuque in IA, USA).

2.2. Apparatus

The UV–vis absorption spectrum was acquired using a UV-1100 UV–vis spectrophotometer (Shimadzu, Japan). The fluorescence spectra were measured on an F-7000 fluorescence spectrophotometer (Hitachi, Japan). Transmission electron microscopy (TEM) was performed using a JEM-2100HR instrument (JEOL Ltd., Japan). The particle size distribution of aptamer conjugated MNPs and MNPs was recorded on zetasizer nano analyser (Malvern Instruments Ltd., England). The experiments were performed using a TriSep™-2100 laser-induced fluorescence detector (Unimicro Technologies company, Shanghai).

2.3. Preparation of aptamer functionalized magnetic nanoparticles

500 μL MNPs (4 mg/mL) was added into 1.5 mL glutaraldehyde solution (2.5 %) and allowed to react in the dark for 2 h. The supernatant was removed using a permanent magnet for magnetic separation, followed by washing with PB buffer (pH 8.0) three times. After adding avidin to react in the dark for 6 h, the mixture was washed with ultrapure water three times. The avidin functionalized magnetic nanoparticles were obtained and stored at 4℃.

The cDNA was heated at 95℃ for 3 min, which was conducive to subsequent hybridization. 240 μL avidin functionalized magnetic nanoparticles were dispersed by ultrasound, and 10 μL cDNA was added to shock incubated at room temperature for 30 min. The unreacted DNA was removed from the supernatant after repeated washing with TE buffer three times, then ultrasonically dispersed in 250 μL TE buffer (pH 8.0) for 3 min. Then 20 μL BSA (1 mg/mL) was added and reacted oscillatory for 1 h, after which the supernatant was removed by magnetic separation. The mixture was then washed with TE buffer three times and dispersed in 250 μL TE buffer to obtain cDNA-modified magnetic nanoparticles (cDNA-MNPs). The scheme of process for cDNA-MNPs is shown in **Fig. S1**. The prepared cDNA-MNPs were stored in a refrigerator at 4℃ for following experiments. Similarly, cApt-29-MNPs and cApt-62-MNPs were prepared by changing the aptamer.

2.4. Measurement procedure

2.4.1. The capillary pretreatment

In order to remove impurities, the quartz capillary was put into the detection cell of laser-induced fluorescence device, and then connected to a 10 mL syringe using a Teflon hose. The syringe was fixed on a syringe pump, and the flow rate was set at 0.08 mL/min. The capillary was pickled with 0.1 mol/L HCl for 2 h, then rinsed with ultrapure water for 30 min, and dried with nitrogen. The capillary aligned with detection cell was burned with fire to remove the coating, making it transparent for laser detection. After each injection, the capillary needed to be cleaned again to ensure the repeatability of the analysis.

2.4.2. The preparation of sample solution

30 μL cDNA-MNPs was ultrasonically dispersed for 3 min to serve as the capture probe, and then tDNA and sDNA with equal volume and certain concentration were added. After mixing, the solution was subjected to water-bath heating at 95℃ for 5 min, and then cooled to room temperature within 1 h to realize hybridization reaction. The preparation of thrombin and *S. aureus* solutions is described in Text S1.

2.4.3. The process of detection

30 μL of mixed solution was drawn up using a micro syringe and placed on the syringe pump. The certain flow rate was set so that the reaction mixture was injected into the quartz capillary through the syringe pump. At the same time, a constant magnetic field was applied to the sample solution for magnetic separation and enrichment. The sample was then washed with a syringe containing TE buffer to remove unreacted impurities until no fluorescent signal appeared. Then, the

magnetic field was removed, and the separated complex was pushed forward using TE buffer at another detection flow rate to make it pass through the detection cell at a uniform speed, and the chromatographic peak was observed at the chromatographic workstation. Under the same conditions, the blank experiment was conducted for detection, and each group performed three parallel experiments.

2.5. The real sample pretreatment

In order to investigate the application of the fabricated equipment, bovine serum was selected as the matrix for real samples. Bovine serum was diluted 50 times (2 % bovine serum), and four thrombin samples with different concentrations (10, 50, 100 and 150 nmol/L) were selected to add standard solution to the diluted samples of fetal bovine serum. Then, the recovery rate of thrombin in the diluted bovine serum sample was determined by contrasting the quantitative curve of thrombin standard.

The practicability of the equipment to detect *S. aureus* was investigated using drinking water and tap water for standard recovery tests. The plate counting was performed on gradient dilution of *S. aureus*. Then, three different concentrations of bacteria suspension were selected within the linear range of the method to detect *S. aureus* and added into drinking water and tap water respectively. Fluorescence detection was carried out by the proposed equipment, and the number of *S. aureus* colonies could be detected in the water samples.

3. Results and discussion

3.1. Design of capillary magnetic separation-DNA equipment

Using capillary as the separation channel and fluid drag force as the driving force, the sandwich structure formed by the hybridization of two DNA probes and tDNA was combined with magnetic nanoparticles for separation and enrichment, and the advantage of highly sensitive detection of laser-induced fluorescence instrument, which realized the integration of separation, enrichment and on-line detection of the samples. As shown in Fig. 1, cDNA-MNPs were used as the capture probe and fluorescence-labeled sDNA served as the signal probe to hybridize with the target, forming a sandwich structure. The mixed solution was injected into the capillary with a syringe fixed on the injection pump. The sandwich structure was fixed by magnetic field force as it passed through the quartz capillary, while impurities and unreacted sDNA generated weak fluorescence signals detected by the laser-induced fluorescence cell. After washing the impurities with buffer, the magnetic field was removed, and cDNA-MNPs-tDNA-sDNA was pushed through the laser-induced fluorescence detection cell at a certain flow rate. The fluorescence signal appeared as a peak on the chromatographic workstation to achieve the purpose of detection for DNA, thrombin and *S. aureus*.

3.2. Characterizations of cDNA functionalized magnetic nanoparticles

The UV–visible absorption spectra of glutaraldehyde, MNPs before and after functionalization are illustrated in Fig. 2A. Glutaraldehyde exhibited strong UV absorption peaks at 233 nm and 280 nm, while MNPs without functionalization did not have such absorption peaks. After functionalization, MNPs showed an obvious UV absorption peak at 240 nm, and the characteristic peaks were red-shifted. Therefore, it can be inferred that glutaraldehyde has successfully reacted with the amino group on the surface of magnetic nanoparticles and the surface has aldehyde groups.

The avidin-modified magnetic nanoparticles were characterized by UV and fluorescence spectroscopy. Fig. 2B shows UV absorption spectra of avidin stock solution and supernatant solution after the reaction of

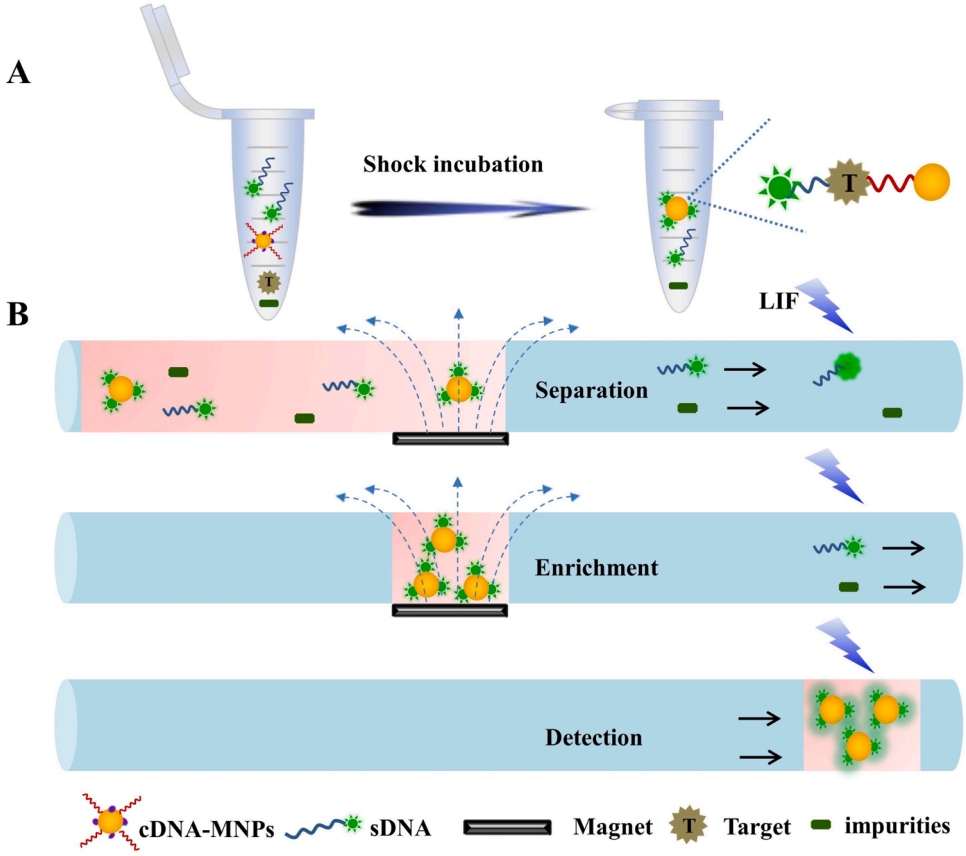

Fig. 1. Scheme of capillary magnetic separation-DNA equipment: (A) The sample pretreatment. (B) The detection process.

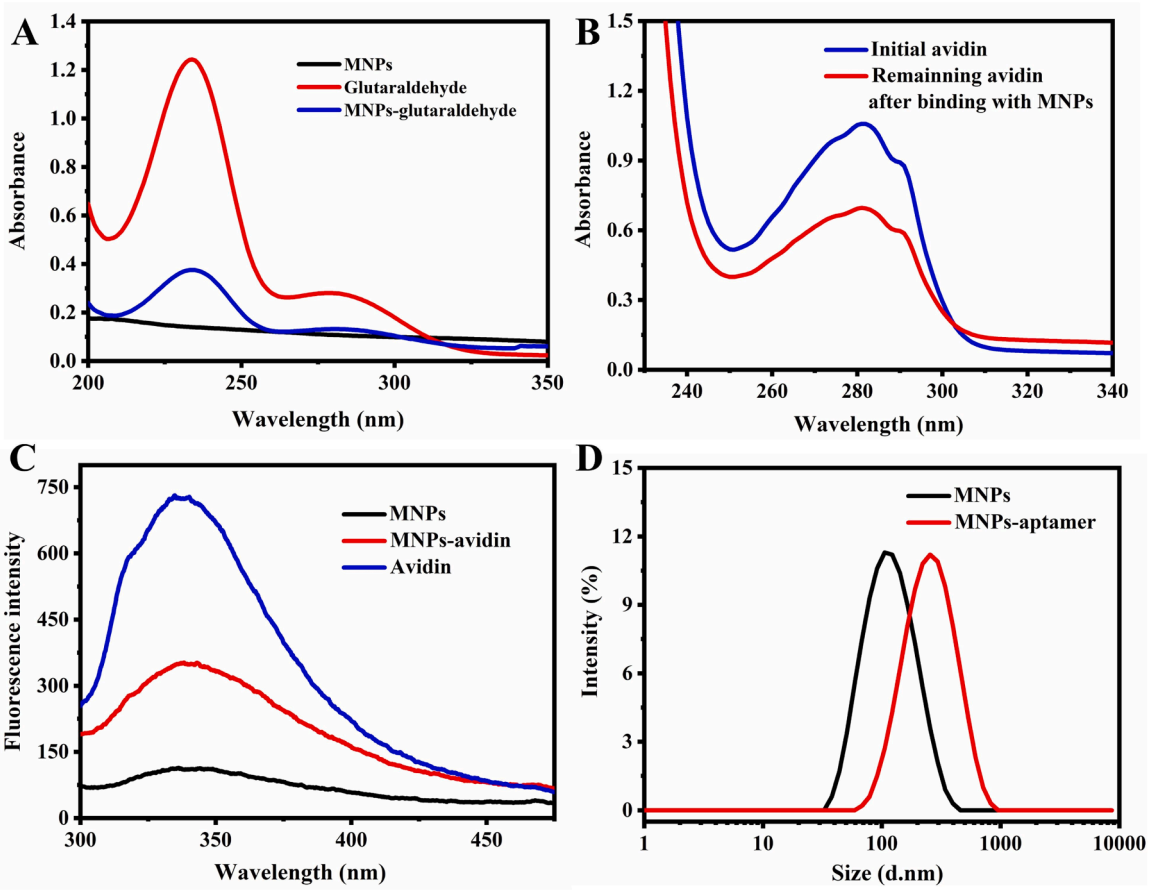

Fig. 2. (A) UV spectra of glutaraldehyde conjugated MNPs. (B) UV spectra and (C) fluorescence spectra of avidin conjugated MNPs. (D) Particle size distribution of cDNA conjugated MNP.

avidin and glutaraldehyde functionalized magnetic nanoparticles. It could be seen that after the incubation of avidin and magnetic nanoparticles, the absorption peak at 280 nm significantly decreased, confirming that avidin and the glutaraldehyde functionalized magnetic nanoparticles were successfully conjugated. As seen in Fig. 2C, avidin had a characteristic fluorescence emission peak at 336 nm, while the magnetic nanoparticles without immobilized avidin did not have this characteristic peak. When the magnetic nanoparticles were modified with the avidin, the characteristic peak appeared at 336 nm, which further confirmed the successful modification of magnetic nanoparticles by avidin.

The particle size distribution of the cDNA-MNPs was analyzed by the nanoparticle size analyzer. The average hydrated particle size of the magnetic nanoparticles was about 100 nm (Fig. 2D). However, after modification with cDNA, it significantly increased to about 250 nm. The dispersion remained stable and had no significant impact on subsequent experiment. Therefore, it was confirmed that biotinylated aptamer, cDNA, specifically bound to the avidin on the surface of magnetic nanoparticles, and the capture probe cDNA was successfully modified on surface of magnetic nanoparticles.

3.3. *Performance of equipment for DNA detection*

BSA is a simple protein in bovine serum, which was used as an enzyme stabilizer or surfactant, and commonly applied in immunoassay for site blocking [37,38]. In this study, BSA was used to reduce the contact between magnetic nanoparticles and FAM, thus reducing the fluorescence quenching effect of magnetic nanoparticles. Meanwhile, BSA could better disperse magnetic nanoparticles, enhancing the sensitivity and repeatability of the method. After adding BSA, the relative fluorescence intensity of the mixture of magnetic nanoparticles and FAM increased from 697 to 930. In order to better play the role of BSA, its concentration is optimized in Fig. 3A. In range of 0.2 ~ 0.8 mg/mL, the final fluorescence peak area increased with rising BSA concentration. However, once the BSA concentration exceeded 0.8 mg/mL, the fluorescence peak area began to decrease as the BSA concentration continued to rise. Therefore, 0.8 mg/mL was determined to be the optimal concentration of BSA.

Due to aggregation of magnetic nanoparticles and physical interaction between magnetic nanoparticles and the capillary, the ideal peak shape cannot be obtained. It is necessary to choose the right flow velocity to generate a certain drag force. Different flow rates (50, 100, 150, 200, 250 μL/min) were set to obtain different fluorescence peaks (Fig. 3B) and fluorescence peak areas (Fig. 3C). Although the fluorescence peak area was large at the flow rate of 50 μL/min, serious tailing could easily cause experimental errors. The peak shape was better and the fluorescence peak area value was relatively high at the flow rate of 150 μL/min, so 150 μL/min was selected as the detection flow velocity.

Magnetic nanoparticles can separate and enrich the target under the force of magnetic field, which is an important part of capillary magnetic separation-DNA equipment. Under a certain volume, an increase in the concentration of magnetic nanoparticles leads to a greater number of particles, thereby enabling the modification of a larger quantity of capture probe cDNA, which could capture a large amount of tDNA and increase the detection range. However, magnetic nanoparticles with a high concentration are more likely to agglomerate, which affects the modification of cDNA and subsequent hybridization with tDNA. In order to obtain the optimal concentration of magnetic nanoparticles, magnetic nanoparticles modified cDNA with the concentration of 0.1, 0.2, 0.3, 0.4, 0.5, 0.6, 0.7, 0.8 mg/mL were selected to detect tDNA. As shown in

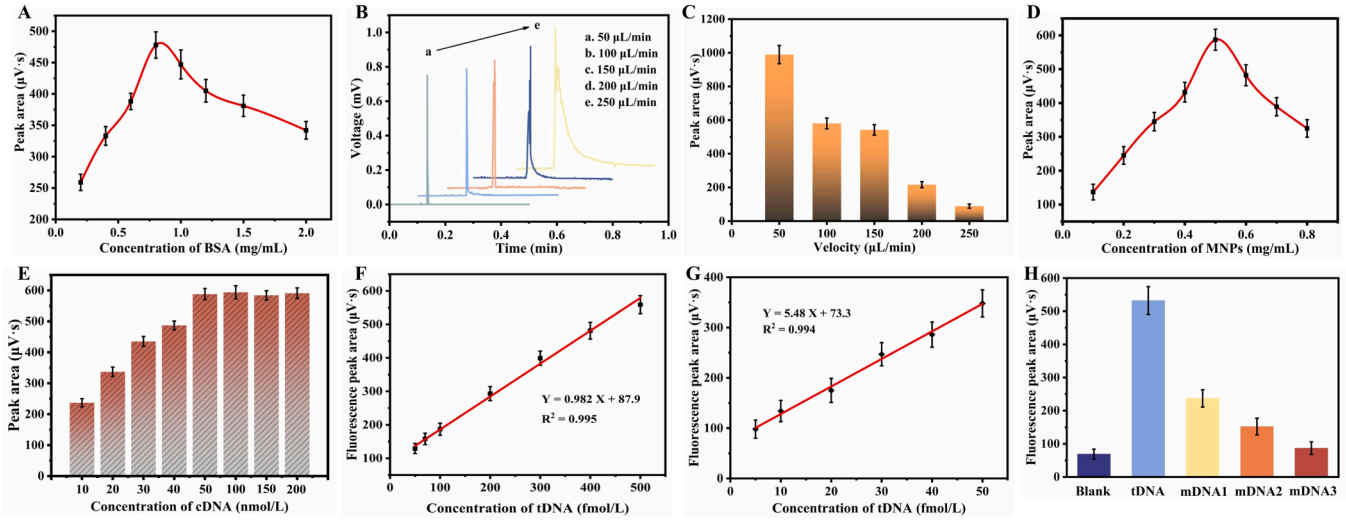

Fig. 3. (A) Effect of BSA concentration on fluorescent peak area. (B) The chromatogram of different velocity. (C) The fluorescence peak area of different velocity. (D) The influence of different concentrations of MNPs. (E) Areas of fluorescence peaks corresponding to different concentrations of cDNA. (F) Calibration curve of tDNA concentration vs fluorescence peak area. (G) The detection of tDNA in 900 μL. (H) The fluorescence peak area of different DNA sequences.

Fig. 3D, the fluorescence peak area reached a maximum at a concentration of 0.5 mg/mL. Therefore, magnetic nanoparticles with a concentration of 0.5 mg/mL were selected for the experiment.

Under the certain concentration of magnetic nanoparticles, the concentration of cDNA affects the quality of cDNA modified onto magnetic nanoparticles. Therefore, the effect of different concentrations of cDNA is investigated in Fig. 3E. Within the range of 10 ~ 50 nmol/L, the final fluorescence peak area value increased with the increase of cDNA concentration. Notably, the fluorescence peak area reached the maximum value at a cDNA concentration of 50 nmol/L, after which the fluorescence peak area no longer changed significantly. Therefore, cDNA with a concentration of 50 nmol/L was selected for subsequent experiments.

Under the optimal experimental conditions, a novel capillary magnetic separation DNA equipment based on laser-induced fluorescence technology was used to quantitatively detect different concentrations of tDNA. Fig. 3F shows the relation curve of different concentration tDNA corresponding fluorescence peak area. Within the range of 50 ~ 500 fmol/L, the fluorescence peak area increased with the increase of tDNA concentration. The linear equation was $Y = 0.982X+87.9$ ($R^2 = 0.995$), and the detection limit was 32.7 fmol/L. The detection method reduced the steps of fixed substrate modification and multiple cleaning. The separation, enrichment and detection were integrated, and the detection process could be finished within 5 min. The detection results of 900 μL reaction system are investigated in Fig. 3G. In the range of 5 ~ 50 fmol/L, the fluorescence peak area and the tDNA concentration had a linear positive correlation. The linear equation was $Y=5.48X+73.3$ ($R^2 = 0.994$) and the detection limit was 2.7 fmol/L.

The specificity of the equipment is based on the specific interaction between the probe and the target, which is an important factor in the qualitative and quantitative detection of the target. Therefore, tDNA and the same concentration (200 fmol/L) of mismatched base DNA sequences (mDNA1, mDNA2, mDNA3) were used to evaluate the specificity of equipment. In Fig. S2, different DNA sequences detected by the equipment to obtain different fluorescence chromatographic peaks. The fluorescence signal of the equipment for target DNA detection was obviously stronger than that of mDNA1, mDNA2 and mDNA3. The fluorescence peak areas of mDNA1, mDNA2 and mDNA3 sequences were 44.5 %, 28.6 % and 16.3 % of tDNA, respectively (Fig. 3H). It could be indicated that the larger the number of base mismatches, the lower the detected fluorescence signal, which was similar to the results reported before [39,40]. Among them, the result of random sequence mDNA3 was similar to the blank control. The above results showed that the mismatch of bases would affect the hybridization with DNA, thus affecting the target DNA captured by functional magnetic nanoparticles and the binding of target DNA to signal probe. This resulted in a weakening of the fluorescence signal, thus ensuring the specificity of equipment for tDNA detection. These results demonstrated that the constructed capillary magnetic separation-DNA equipment had excellent specificity.

3.4. Feasibility of thrombin detection and analytical performance

In this study, capillary magnetic separation-DNA equipment was applied to the detection of thrombin, mainly based on the principle of specific binding of thrombin and its aptamer. Therefore, it is very important that the prepared cApt-29-MNPs can successfully capture thrombin for the subsequent experiment. The Coomassie brilliant blue method has high sensitivity, fast and simple determination, fewer interferences, stable color and easy observation [41]. It can meet the requirements for rapid qualitative detection of micro-thrombin and realize qualitative colorimetry with naked eyes. Therefore, the Coomassie brilliant blue method was chosen to verify successful capture of thrombin by cApt-29-MNPs.

The Coomassie brilliant blue G-250 has red color in the free state, with the maximum light absorption at a wavelength of 488 nm. It turns cyan when combined with protein, and the maximum absorption wavelength of protein-pigment conjugate is 595 nm. The thrombin solution was mixed and incubated with cApt-29-MNPs, then the unreacted solution was removed by magnetic separation and the blank control group was set with no thrombin added. The complex obtained after reaction was reacted with Coomassie brilliant blue G-250 for 2 min and then detected by UV spectrophotometer. As shown in Fig. S3, both the experimental group and the blank group had absorption peaks at the wavelengths of 458 nm and 643 nm. This may be due to the addition of BSA during the preparation of cApt-29-MNPs, and the combination of BSA and Coomassie brilliant blue G-250 resulted in an absorption peak at 643 nm in the sample solution. The presence of DNA and magnetic nanoparticles in cApt-29-MNPs resulted in red shift or blue shift of the maximum absorption peak wavelength. Compared with the blank group, the absorption value at 458 nm decreased in the experimental group, while the absorption value at 643 nm increased. In addition, the experimental group in the inset of Fig. S3 was darker than the blank group. Therefore, these results confirmed that cApt-29-MNPs have

successfully captured thrombin.

The two thrombin aptamers, cApt-29 and sApt-15, were used to recognize the heparin binding site of thrombin and the fibrinogen binding site, respectively. These two aptamers both contain G-quadruplex structure, and the specific effect of the aptamer and thrombin is related to the formation of G-quadruplex. Studies have shown that the presence of K^+ contributes to the stabilization of G-quadruplex structure of the aptamer, and Mg^{2+} has a stabilizing effect on the double-stranded DNA structure, thus promoting the formation of G-quadruplexes [42]. Therefore, the effects of different concentrations of K^+ and Mg^{2+} in buffer on the detection of thrombin by equipment were investigated.

As shown in Fig. 4A, when the concentration of thrombin was 200 nmol/L, the fluorescence peak area decreased with the presence of K^+ and Mg^{2+} in the buffer. With the increase of concentration of K^+ or Mg^{2+} in the buffer, the value of the fluorescence peak area decreased. This indicated that both K^+ and Mg^{2+} have a negative effect on the detection results. The possible reason was that the presence of salt ions changed the surface charge of the magnetic nanoparticles, prompting them to agglomerate and affecting the detection results. Therefore, Tris-HCl buffer (pH 7.4) without salt ions was used as the sample solvent and separation buffer in subsequent experiments.

The combination of thrombin and aptamer is an important factor to affect the detection of thrombin. The higher the binding rate, the more thrombin can be captured by the capturing probe, and the higher the number of signal probes, thereby increasing the sensitivity of detection and reducing the detection limit. In order to obtain the optimal time for incubation, 200 nmol/L thrombin sample was reacted with cApt-29-MNPs and sApt-25 for 10, 30, 60, 90, 120 and 240 min at room temperature for fluorescence detection. As depicted in Fig. 4B, the peak area of fluorescence increased along with the incubation time. The change of fluorescence peak area was no longer obvious when the incubation time reached 60 min, indicating that the binding of thrombin and aptamer

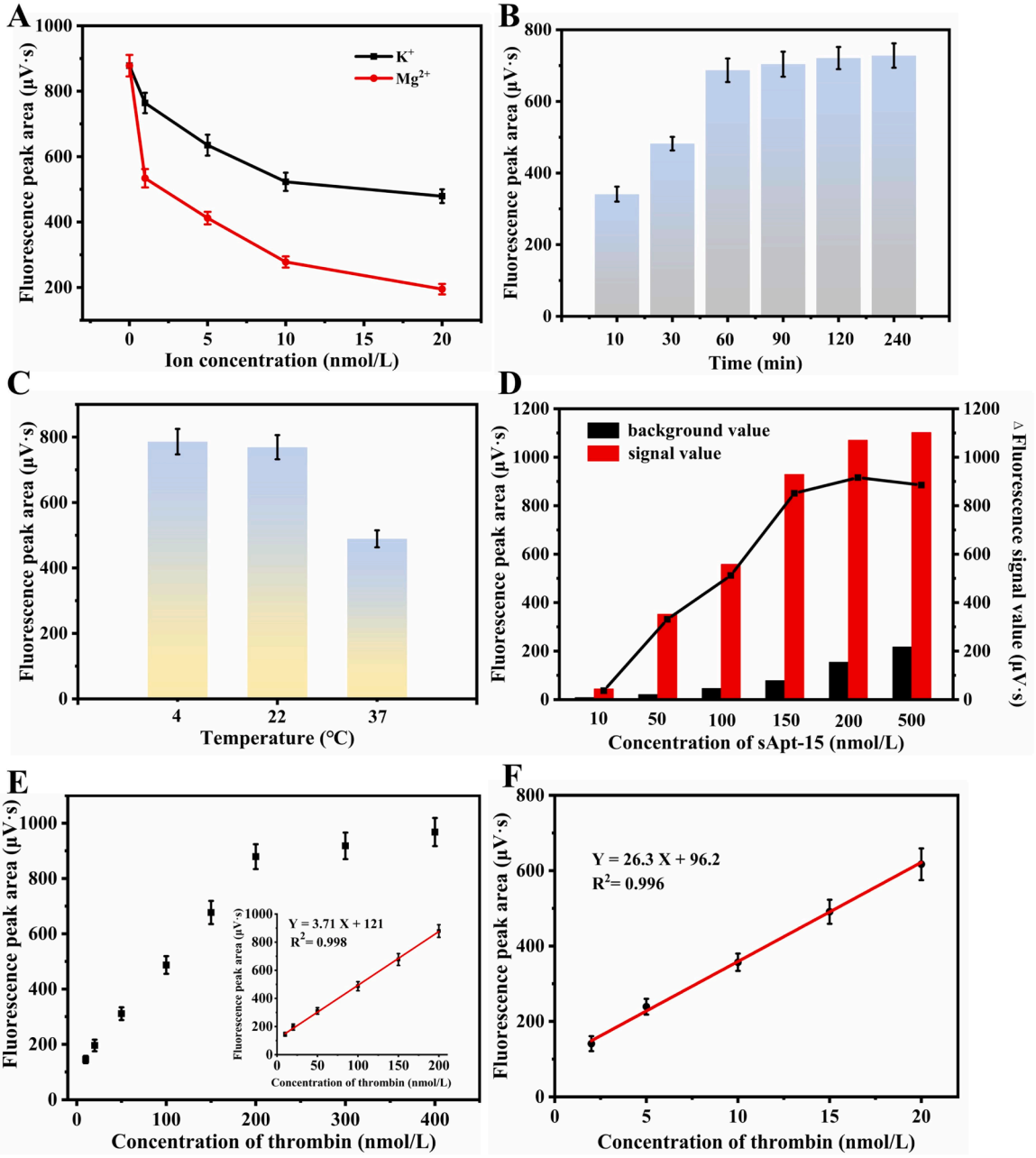

Fig. 4. (A) Effect of the concentration of K^+ and Mg^{2+}. (B) Optimization of incubation time of thrombin with aptamer. (C) Fluorescence peak area of thrombin in 4°C, 22°C (room temperature) and 37°C. (D) Effect of the concentration of sApt-15. Calibration curves of different concentration of thrombin (E) 90 μL (F) 900 μL.

reached satiation. In order to improve detection performance, 60 min was selected as the optimal incubation time.

The incubation temperature required for the reaction between thrombin and aptamer is significant for detection. 200 nmol/L thrombin sample was reacted with cApt-29-MNPs and sApt-25 at 4°C, 22°C (room temperature) and 37°C (water bath) for 60 min for fluorescence detection. In Fig. 4C, the maximum fluorescence peak area was obtained at 4℃. It suggested that 4°C is more conducive to the detection of thrombin. Nevertheless, there was little difference between 22°C (room temperature) and 4°C. Therefore, room temperature was selected as the incubation temperature in this experiment for operation convenience and cost savings.

The effect of sApt-15 concentration was also investigated. 200 nmol/L thrombin sample was mixed with cApt-29-MNPs and different concentrations of sApt-25 (10, 50, 100, 150, 200, 500 nmol/L) at room temperature for 60 min to perform fluorescence detection. The fluorescence signal gradually increased with the increase of sApt-15 concentration (Fig. 4D). When the concentration reached 200 nmol/L, the area of the fluorescence peak did not increase significantly, demonstrating that the combination of sApt-15 and thrombin has reached a

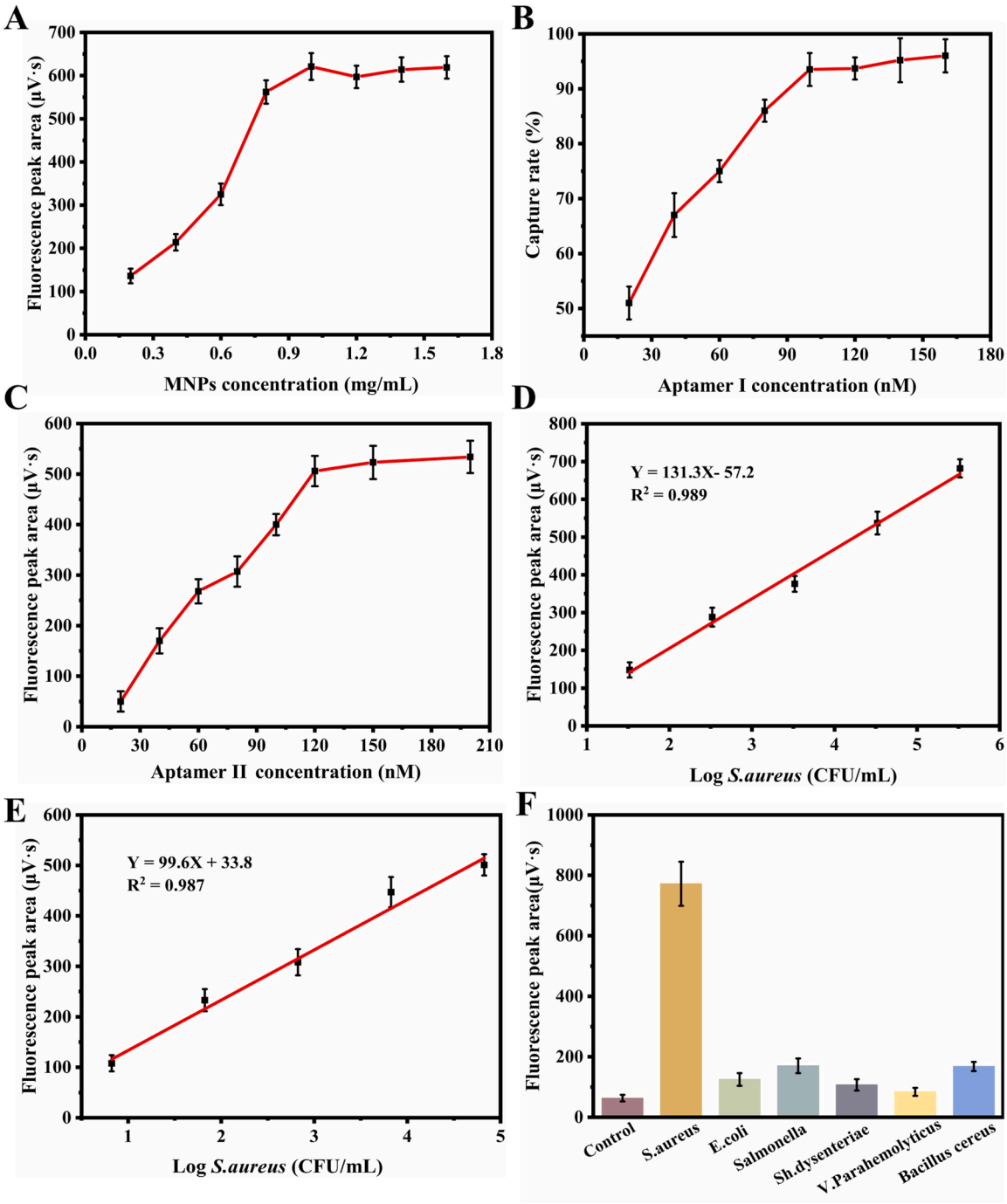

Fig. 5. (A) Effect of MNPs concentration on fluorescent peak area. (B) Effect of biotin-aptamer I concentration on bacteria capture rate. (C) Effect of FAM-Aptamer II concentration on fluorescent peak area. Calibration curves of detecting different concentration of *S. aureus* (D) 90 μL (E) 450 μL. (F) The specificity analysis of the proposed method (Bacterial concentrations were 3.3×10^4 CFU/mL, 2.4×10^4 CFU/mL, 3.2×10^4 CFU/mL, 2.3×10^4 CFU/mL, 1.6×10^4 CFU/mL, 2.7×10^4 CFU/mL, respectively).

saturated state. Although the addition of BSA in the preparation of cApt-29-MNPs played a passivation effect, it did not completely eliminate non-specific adsorption. With the increase of sApt-15 concentration, background signal also increased rapidly. Therefore, the difference between 150 nmol/L and 200 nmol/L sApt-15 concentration was not obvious after the background value was subtracted from the signal value for comparison. In order to save costs, 150 nmol/L sApt-15 concentration of signal probe was selected in the experiment.

Under the optimal experimental conditions, different concentrations of thrombin were detected by DNA equipment. In Fig. 4E, in the range of 10 ~ 200 nmol/L, the fluorescence peak area obtained by detection was linearly correlated with the thrombin concentration. The linear equation was Y=3.71X+121 (R^2=0.998) and the detection limit was 9.7 nmol/L (the corresponding sample solution volume was 90 μL). However, with the continuous increase of thrombin concentration, the increase of fluorescence peak area was no longer obvious and tended to be stable. It may be because under certain conditions of the amount of cApt-29-MNPs and sApt-15, when the concentration of thrombin was high, the binding of the probe and thrombin reached saturation. The excess thrombin was no longer captured or produced fluorescent signal, which showed that the fluorescence peak area tended to be stable. As shown in Fig. 4F, the linear equation was Y= 26.3X+96.2 (R^2=0.996) and the detection limit was 0.57 nmol/L (the corresponding sample solution volume was 900 μL).

The performance of capillary magnetic separation-DNA equipment for thrombin detection in complex sample substrates was investigated using the diluted bovine serum as the sample substrate. In Table S2, the recovery rate of thrombin in the 50-fold diluted bovine serum ranged from 87.5 % to 97.3 %, indicating that the equipment has the prospect of practical application.

3.5. Analytical performance of DNA equipment for S. aureus detection

TEM images of cApt-62-MNPs and cApt-62-MNPs combined with *S. aureus* are shown in Fig.S4. In Fig. S4A, the particle size of MNPs was about 10 nm and the dispersion was relatively uniform. Fig. S4B shows that the diameter of *S. aureus* was about 600 nm. It could be concluded that cApt-62-MNPs successfully binds to the surface of *S. aureus*, further confirming that cApt-62-MNPs can be used to capture *S. aureus*, and can be separated and enriched by using magnetic characteristics.

To achieve desirable analytical characteristics, the effect of concentration of the MNPs probe is investigated in Fig. 5A. The fluorescence peak area increased with the increase of the MNPs concentration, reaching its maximum at a concentration of 1.0 mg/mL and no longer changing thereafter. Therefore, the optimal concentration of MNPs was 1.0 mg/mL. The concentration of aptamer I and aptamer II were optimized for both capture probe and signal probe. In Fig. 5B, after coupling with MNPs, aptamer I (cApt-62) was used to capture *S. aureus* from the sample. Increasing the loading of aptamer I on MNPs can increase the affinity and quantity of aptamer I available for binding to *S. aureus*, ultimately improving the capture efficiency. With increasing concentration of biotin-aptamer I, the capture rate of *S. aureus* increased first and reached the maximum at 93 %. Hence, the concentration of biotin-aptamer I was chosen as 100 nmol/L. As observed in Fig. 5C, various concentrations of FAM-aptamer II (sApt-62) as signal probe were added to determine the optimal concentration. The fluorescence peak area grew rapidly as the concentration of the FAM-aptamer II increased from 20 nmol/L to 120 nmol/L, but remained steady when the concentration exceeded 120 nmol/L, indicating the binding between aptamer and *S. aureus* had reached the saturation. Therefore, 120 nmol/L was chosen as the optimal concentration of FAM-aptamer II for further experiments.

Under the optimal conditions, the equipment accurately established the correlation between the concentration of *S. aureus* and the fluorescence peak area. As shown in Fig. 5D, when the total reaction volume was 90 μL, within the range of 3.3×10^1 ~ 3.3×10^5 CFU/mL, *S. aureus* concentration had a good linear relationship with fluorescence peak area. The linear equation was Y= 131.3X-57.2 (R^2=0.989) and the detection limit was 8 CFU/mL. In Fig. 5E, when the total volume of the reaction system increased from 90 μL to 450 μL, the linear range was 6.7 ~ 6.7×10^4 CFU/mL. The linear equation was Y= 99.6X+33.8 (R^2=0.987), and the detection limit was 3 CFU/mL. The performance of the proposed detection method was compared with other reported works, and the results were summarized in Table S3. The comparison shows that the proposed method has wide linear range, high sensitivity and short detection time, which proves the effectiveness for sensitive and rapid detection of multiple biomolecules.

In order to verify the specificity of the equipment, *S. aureus*, *E. coli*, *Salmonella*, *Shigella dysenteriae*, *Vibrio parahaemolyticus* and *Bacillus cereus* were investigated, and TE buffer was used as blank control for comparison. As seen from Fig. 5F, the fluorescence signal of *S. aureus* was stronger than other bacteria. The result indicated that the equipment had good specificity for *S. aureus*.

In order to verify the practicability of this method, *S. aureus* was diluted into different gradient concentrations of bacterial suspensions after ultraviolet irradiation sterilization of bottled water and tap water. The results obtained from the standard curve were compared with those obtained by the plate counting method. As shown in Table S4, the results obtained by two methods are similar, indicating that the fabricated equipment has the potential for detecting *S. aureus* in practical samples.

4. Conclusion

In this study, the integration of separation, enrichment, and on-line detection was achieved in capillary combined with laser-induced fluorescence. The detection target has been expanded from DNA to proteins and pathogenic bacteria, broadening the application ranges. This method has the advantages of high specificity and simple operation, and can realize rapid separation, enrichment and detection. It provides a promising tool for on-line detection of trace substances and expands the potential applications in environment detection and disease diagnosis.

CRediT authorship contribution statement

Shu-Ting Cheng: Writing – original draft, Investigation, Formal analysis, Conceptualization. **Rong-Rong Meng:** Methodology, Investigation, Formal analysis. **Yue-Hong Pang:** Writing – review & editing, Methodology. **Xiaofang Shen:** Supervision, Project administration, Funding acquisition.

Declaration of Competing Interest

The authors declare that they have no known competing financial interests personal relationships that could have appeared to influence the work reported in this paper.

Acknowledgements

This work was supported by the National Key Research and Development Program of China (2022YFF1100803), and the National Natural Science Foundation of China (22476068).

Appendix A. Supporting information

Supplementary data associated with this article can be found in the online version at doi:10.1016/j.snb.2024.136840.

Data availability

Data will be made available on request.

References

[1] R.S. Juang, W.T. Chen, Y.W. Cheng, K.S. Wang, R.J. Jeng, Z.L. Zeng, S.H. Liu, T. Y. Liu, Fabrication of in situ magnetic capturing and Raman enhancing nanoplatelets for detection of bacteria and biomolecules, Colloid Surf. A. 648 (2022) 129189.

[2] X. Zhang, Y. Shi, D. Wu, L. Fan, J. Liu, Y. Wu, G. Li, A bifunctional core-shell gold@Prussian blue nanozyme enabling dual-readout microfluidic immunoassay of food allergic protein, Food Chem. 434 (2024) 137455.

[3] J. Zheng, X. Fang, L. Li, R. Zhang, C. Li, Biomolecule-responsive nanoprobes for living cell analysis, Trac-Trend Anal. Chem. 169 (2023) 117387.

[4] H. Yang, Y. Zhang, X. Teng, H. Hou, R. Deng, J. Li, CRISPR-based nucleic acid diagnostics for pathogens, Trac-trend, Anal. Chem. 160 (2023) 116980.

[5] H. Bai, Y. Wang, X. Li, J. Guo, Electrochemical nucleic acid sensors: competent pathways for mobile molecular diagnostics, Biosens. Bioelectron. 237 (2023) 115407.

[6] J. Huang, W. Ma, H. Sun, H. Wang, X. He, H. Cheng, M. Huang, Y. Lei, K. Wang, Self-assembled DNA nanostructures-based nanocarriers enabled functional nucleic acids delivery, ACS Appl. Bio Mater. 3 (2020) 2779–2795.

[7] L. Zhang, B. Ding, Q. Chen, Q. Feng, L. Lin, J. Sun, Point-of-care-testing of nucleic acids by microfluidics, Trac-Trend Anal. Chem. 94 (2017) 106–116.

[8] J. Zhu, X. Qu, Y. Zhuang, P. Miao, Entropy-driven strand displacements around DNA tetrahedron for sensitive detection and intracellular imaging of mRNA, Small Struct. 5 (2024) 2300420.

[9] Y. Zhao, Y. Zhao, Y. Sun, L. Fan, D. Wang, H. Wang, X. Sun, Z. Zheng, A direct, sensitive and high-throughput genus and species-specific molecular assay for large-scale malaria screening, Infect. Dis. Poverty 11 (2022) 25.

[10] J. Liang, L. Wu, Y. Wang, W. Liang, Y. Hao, M. Tan, G. He, D. Lv, Z. Wang, T. Zeng, X. Zhang, C. Lu, Q. Song, B. Peng, J. Zhao, B. Zhu, Y. Tang, SERS/photothermal-based dual-modal lateral flow immunoassays for sensitive and simultaneous antigen detection of respiratory viral infections, Sens. Actuator B: Chem. 389 (2023) 133875.

[11] M. Lin, P. Song, G. Zhou, X. Zuo, A. Aldalbahi, X. Lou, J. Shi, C. Fan, Electrochemical detection of nucleic acids, proteins, small molecules and cells using a DNA-nanostructure-based universal biosensing platform, Nat. Protoc. 11 (2016) 1244–1263.

[12] P. Alinezhad, H. Staji, R.N. Sani, Comparison of three methods including temperature, H_2O_2/ascorbic acid/sonication, and nitrous acid treatments for overcoming the inhibitory effect of heparin on DNA amplification in realtime-PCR, Int. J. Biol. Macromol. 209 (2022) 1298–1306.

[13] B.S. Alladin-Mustan, Y. Liu, Y. Li, D.R.Q. de Almeida, J. Yuzik, C.F. Mendes, J. M. Gibbs, Reverse transcription lesion-induced DNA amplification: an instrument-free isothermal method to detect RNA, Anal. Chim. Acta 1149 (2021) 238130.

[14] Y. Wang, Y. Fei, T. Yang, Z. Luo, Y. Xu, B. Su, X. Lin, Nanotechnology for ultrafast nucleic acid amplification, Nano Today 48 (2023) 101749.

[15] K. Salimi, D.D. Usta, I. Kocer, E. Celik, A. Tuncel, Protein A and protein A/G coupled magnetic SiO_2 microspheres for affinity purification of immunoglobulin G, Int. J. Biol. Macromol. 111 (2018) 178–185.

[16] J. Du, D. Xiang, F. Liu, L. Wang, H. Li, L. Gong, X. Fan, Hijacking the self-replicating machine of bacteriophage for PCR-based cascade signal amplification in detecting SARS-CoV-2 viral marker protein in serum, Sens. Actuator B: Chem. 374 (2023) 132780.

[17] J. Zhang, L. Hao, Z. Zhao, D. Jiang, J. Chao, Multiple signal amplification electrochemiluminescence biosensor for ultra-sensitive detection of exosomes, Sens. Actuator B: Chem. 369 (2022) 132332.

[18] H. Fu, Z. Bai, P. Li, X. Feng, X. Hu, X. Song, L. Chen, Molecular imprinted electrochemical sensor for ovalbumin detection based on boronate affinity and signal amplification approach, Food Chem. 409 (2023) 135292.

[19] Y. Zheng, X. Cui, Y. Zhou, H. Zhang, L. Cao, L. Gao, H. Yin, S. Ai, MXene enhanced photoactivity of Bi_2O_3/Bi_2S_3 heterojunction with G-wire superstructure for photoelectrochemical detection of TET1 protein, ACS Sens 7 (2022) 3116–3125.

[20] J. Sun, J. Huang, Y. Li, J. Lv, X. Ding, A simple and rapid colorimetric bacteria detection method based on bacterial inhibition of glucose oxidase-catalyzed reaction, Talanta 197 (2019) 304–309.

[21] Q. Li, Y. Wu, H. Lu, X. Wu, S. Chen, N. Song, Y.W. Yang, H. Gao, Construction of supramolecular nanoassembly for responsive bacterial elimination and effective bacterial detection, ACS Appl. Mater. Interfaces 9 (2017) 10180–10189.

[22] W.H. Yu, Z.L. Qiu, J.R. Wang, Y.J. Shen, J. Han, L.F. Fang, B.K. Zhu, Novel nanofiltration membrane prepared by amphiphilic random copolymer nanoparticles packing for high-efficiency biomolecules separation, Chem. Eng. J. 430 (2022) 132914.

[23] C.L. Crihfield, L.A. Holland, Protein sieving with capillary nanogel electrophoresis, Anal. Chem. 93 (2021) 1537–1543.

[24] Q. Wang, K. Peng, N. Gan, X. Liu, H. Huang, H. Shao, H. Jin, J. Crommen, Z. Jiang, Rapid fabrication of versatile zwitterionic super-hydrophilic polymers by sole-monomer system for biomolecules separation, Chem. Eng. J. 396 (2020) 125121.

[25] G. Cecile Urbain Marie, V. Perreault, L. Henaux, V. Carnovale, R.E. Aluko, A. Marette, A. Doyen, L. Bazinet, Impact of a high hydrostatic pressure pretreatment on the separation of bioactive peptides from flaxseed protein hydrolysates by electrodialysis with ultrafiltration membranes, Sep. Purif. Technol. 211 (2019) 242–251.

[26] H.G. Lee, J.Y. Kwon, D.S. Chung, Sensitive arsenic speciation by capillary electrophoresis using UV absorbance detection with on-line sample preconcentration techniques, Talanta 181 (2018) 366–372.

[27] N.V.T. Nguyen, C. Smadja, M. Taverna, S.El Mousli, E. Secret, J.M. Siaugue, L.T. H. Nguyen, T.D. Mai, Electroosmotic flow modulation for improved electrokinetic preconcentration: Application to capillary electrophoresis of fluorescent magnetic nanoparticles, Anal. Chim. Acta 1161 (2021) 338466.

[28] Y. Liang, J.L. Gong, Y. Huang, Y. Zheng, J.H. Jiang, G.L. Shen, R.Q. Yu, Biocompatible core-shell nanoparticle-based surface-enhanced Raman scattering probes for detection of DNA related to HIV gene using silica-coated magnetic nanoparticles as separation tools, Talanta 72 (2007) 443–449.

[29] W. Zhao, D. Zhang, T. Zhou, J. Huang, Y. Wang, B. Li, L. Chen, J. Yang, Y. Liu, Aptamer-conjugated magnetic Fe_3O_4@Au core-shell multifunctional nanoprobe: a three-in-one aptasensor for selective capture, sensitive SERS detection and efficient near-infrared light triggered photothermal therapy of Staphylococcus aureus, Sens. Actuator B: Chem. 350 (2022) 130879.

[30] X. Du, Q. He, L. Zhang, C. Liu, J. Zhu, B. Kuang, S. Zeng, B. Chen, D. Yin, Y. Zeng, Selective and cleavable extraction of sialo-glycoproteins by disulfide-linked amino-oxy-functionalized Fe_3O_4 magnetic nanoparticles, Bioconjug. Chem. 28 (2017) 2514–2517.

[31] H. Zhang, Y. Liu, K. Zhang, J. Ji, J. Liu, B. Liu, Single molecule fluorescent colocalization of split aptamers for ultrasensitive detection of biomolecules, Anal. Chem. 90 (2018) 9315–9321.

[32] L. Moran, N. Aldai, L.J.R. Barron, Elucidating the combined effect of sample preparation and solid-phase microextraction conditions on the volatile composition of cooked meat analyzed by capillary gas chromatography coupled with mass spectrometry, Food Chem. 352 (2021) 129380.

[33] L. Huang, M. Fang, K.A. Cupp-Sutton, Z. Wang, K. Smith, S. Wu, Spray-capillary-based capillary electrophoresis mass spectrometry for metabolite analysis in single cells, Anal. Chem. 93 (2021) 4479–4487.

[34] Y. Wang, J. Wu, P. Sun, J. Yu, Q. Pu, A fully functional palmtop microchip electrophoresis analyzer with laser-induced fluorescence detection, Sens. Actuator B: Chem. 372 (2022) 132645.

[35] Q. Xi, M. Shi, X. Geng, X. Wang, Y. Guan, Spherical dichroic reflector improves limit of detection in laser-induced fluorescence detection, Anal. Chem. 92 (2020) 8680–8684.

[36] L. Sun, Y. Li, H. Wang, Q. Zhao, An aptamer assay for aflatoxin B1 detection using Mg^{2+} mediated free zone capillary electrophoresis coupled with laser induced fluorescence, Talanta 204 (2019) 182–188.

[37] M.M. Habibi, S.A. Mirhosseini, S. Sajjadi, A.H. Keihan, A novel label-free electrochemical immunesensor for ultrasensitive detection of LT toxin using prussian blue@gold nanoparticles composite as a signal amplification, Bioelectrochemistry 142 (2021) 107887.

[38] M. Szymanska, I. Pospieszna-Markiewicz, M. Manka, M. Insinska-Rak, G. Dutkiewicz, V. Patroniak, M.A. Fik-Jaskolka, Synthesis and spectroscopic investigations of schiff base ligand and its bimetallic Ag(I) complex as DNA and BSA binders, Biomolecules 11 (2021) 1449.

[39] Y. Huang, H.Y. Yang, Y. Ai, DNA single-base mismatch study using graphene oxide nanosheets-based fluorometric biosensors, Anal. Chem. 87 (2015) 9132–9136.

[40] M. Shi, J. Zheng, Y. Tan, G. Tan, J. Li, Y. Li, X. Li, Z. Zhou, R. Yang, Ultrasensitive detection of single nucleotide polymorphism in human mitochondrial DNA utilizing ion-mediated cascade surface-enhanced raman spectroscopy amplification, Anal. Chem. 87 (2015) 2734–2740.

[41] H. Zhang, L. Wang, X. Yao, Z. Wang, L. Dou, L. Su, M. Zhao, J. Sun, D. Zhang, J. Wang, Developing a simple immunochromatography assay for clenbuterol with sensitivity by one-step staining, J. Agric. Food Chem. 68 (2020) 15509–15515.

[42] Y. Cao, W. Li, P. Ding, R. Pei, Acid-facilitated G-quadruplex/hemin DNAzymes: accompanied by the assembly of quadruplex supramolecules, Chem. Commun. 56 (2020) 8667–8670.

Shu-Ting Cheng is currently studying for her Ph.D. degree in School of Food Science and Technology, Jiangnan University, China. Her research focuses on the construction of aptasensor and their application in food hazards detection.

Rong-Rong Meng is a master student supervised by Prof. Xiao-Fang Shen at School of Food Science and Technology, Jiangnan University, China. Her research focuses on the application of new methods for food safety.

Yue-Hong Pang is currently a professor in Jiangnan University, China. Her research interests include the fabrication of novel nanomaterials and their application for electrochemical sensors.

Xiao-Fang Shen is currently a professor in Jiangnan University, China. His main research interests are in food safety detection, bioassay, nanotechnology and biological sensing